IC/87/292

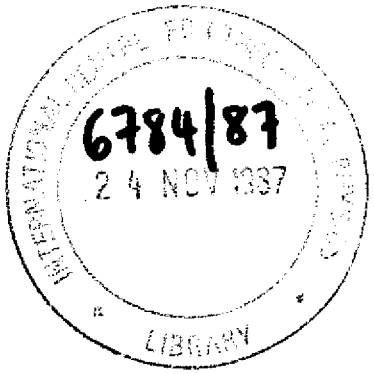

INTERNATIONAL CENTRE FOR THEORETICAL PHYSICS

MODE COUPLING ANALYSIS
OF COHERENT QUASI-ELASTIC NEUTRON SCATTERING
FROM FLUORITE-TYPE MATERIALS
APPROACHING THE SUPERIONIC TRANSITION

D.K. Chaturvedi

and

M.P. Tosi

INTERNATIONAL ATOMIC ENERGY AGENCY

UNITED NATIONS EDUCATIONAL, SCIENTIFIC AND CULTURAL ORGANIZATION

1987 MIRAMARE-TRIESTE

International Atomic Energy Agency
and
United Nations Educational Scientific and Cultural Organization

INTERNATIONAL CENTRE FOR THEORETICAL PHYSICS

MODE COUPLING ANALYSIS OF COHERENT QUASI-ELASTIC NEUTRON SCATTERING FROM FLUORITE-TYPE MATERIALS APPROACHING THE SUPERIONIC TRANSITION *

D.K. Chaturvedi **
International Centre for Theoretical Physics, Trieste, Italy
and
Physics Department, Kurukshetra University,
Kurukshetra 132119, India

and

M.P. Tosi
International Centre for Theoretical Physics, Trieste, Italy
and
Dipartimento di Fisica Teorica, University di Trieste,
Trieste, Italy.

MIRAMARE - TRIESTE
August 1987

* Submitted for publication.

Abstract Neutron scattering experiments on $SrCl_2$, CaF_2 and PbF_2 have shown that intensity and width of the coherent diffuse quasi-elastic spectrum increase rapidly with temperature into the fast-ion conducting phase, the main feature in the integrated quasi-elastic intensity being a peak just beyond the (200) point along the [100] direction in scattering wave vector space. The Zwanzig-Mori memory function formalism is used in this work to analyze the quasi-elastic scattering cross section from charge density fluctuations in terms of anharmonic couplings between the vibrational modes of the crystal. The two- and three-mode channels are examined for compatibility with the quasi-elastic neutron scattering evidence, on the basis of (i) energy and momentum conservation and van Hove singularity arguments and (ii) measured phonon dispersion curves along the main symmetry directions in $SrCl_2$, CaF_2, SrF_2 and BaF_2. The analysis identifies a specific microscopic role for the Raman-active optic branches. The eigenvectors of the relevant Raman-active and partner modes in the three-mode channel describe relative displacements of the two halogens in the unit cell superposed on relative displacements of the halogen and alkaline earth components. This microscopic picture is thus consistent with the superionic transition being associated with the onset of dynamic disorder in the anionic component of the crystal.

1. Introduction

A diffuse transition to a state of high electric conductivity by anions occurs in fluorite-structure materials over a range of temperature without changes in crystal structure. Inelastic coherent neutron scattering experiments[1] and Raman scattering experiments[2] show that the optic and high-energy acoustic vibrational modes broaden rapidly with increasing temperature across the transition. An additional observed effect of dynamic anionic disorder is the appearance and growth of coherent quasi-elastic diffuse scattering[3,4] (QES). The QES spectrum is well described by a Lorentzian scattering function $S(\mathbf{k},\omega)$ centred at transferred energy $\omega = 0$ and varying strongly with scattering wave vector $\mathbf{k}$. Its integrated intensity yields a structure factor $S(\mathbf{k})$ which is mainly concentrated on an anisotropic shell in wave vector space, with a prominent peak in the region $\mathbf{k} = (2\pi/a)(2.2 - 2.4, 0, 0)$ depending on the material (CaF_2, PbF_2 or $SrCl_2$).

It is natural to associate the observed QES spectrum with the rapidly rising ionic conductivity across the superionic transition and thus to look for its interpretation as the low-frequency part of the spectrum of correlations between microscopic charge density fluctuations in the material. The measured $S(\mathbf{k},\omega)$ is in this view simply proportional to the imaginary part of the inverse of the dielectric function $\varepsilon(\mathbf{k},\omega)$ and hence directly proportional to the real part of the longitudinal non-local electric conductivity $\sigma(\mathbf{k},\omega)$, at frequencies ω which are low compared with phonon frequencies. The latter function is analyzed in this work by means of the Zwanzig-Mori memory function formalism[5] in a mode coupling approximation.

The microscopic ionic dynamics has been previously evaluated for a symmetric model of molten salts near freezing with the help of the memory function formalism in a two-mode coupling approximation, which allows approximate selfconsistent calculations of the relevant correlation spectra[6-8]. In the case of superionic fluorites, however, it is soon seen that three-mode decay processes can contribute to the main observed characteristics of the QES. We are nevertheless able to make some progress

without carrying out prohibitively complex calculations if we neglect selfconsistency and represent the spectral functions of the modes entering the memory function as those of ideal undamped vibrations. Simple considerations of energy and momentum conservation and of densities of vibrational states can then be applied to restrict the search for the modes that may be expected to intervene in determining the microscopic ionic conductivity. Evidently, our discussion is limited to the onset of anionic disorder leading into the fast-ion conducting state.

The theoretical approach that we have sketched above is developed in section 2 of the paper. In section 3 we proceed to examine measured phonon dispersion curves along the main symmetry directions in fluorite-type systems showing a superionic transition at high temperature ($SrCl_2$[9], CaF_2[10], SrF_2[11] and BaF_2[12]). A few alternative three-mode processes appear to be compatible with the observed QES, a Raman-active optic mode being involved, however, in all cases. Calculations of the relevant mode eigenvectors are also reported in this section, in order to ascertain the nature of the microscopic atomic displacements. The implications of the results are discussed in section 4 of the paper.

2. Nonlocal conductivity in mode coupling approximations

Following the earlier discussions of ionic dynamics in a symmetric model of molten salts[6-8], we write the real part of the microscopic longitudinal conductivity $\sigma(\mathbf{k},\omega)$ as directly proportional to the imaginary part of a memory function $M(\mathbf{k},\omega)$, defined through the Laplace transform of the correlation function of fluctuating forces which perturb the secular motion of the longitudinal electric current density. In a mode coupling treatment we expand the memory function into processes that involve successively higher numbers of coupled modes,

$$\mathrm{Re}\,\sigma(\mathbf{k},\omega) \propto \sum_{n=2}^{\infty} \mathrm{Im}\,M_n(\mathbf{k},\omega) \qquad (2.1)$$

We explicitly have for the two-mode and three-mode processes the expressions

$$\mathrm{Im}\, M_2(\mathbf{k},\omega) = \sum_{\alpha,\beta} \int\int d\mathbf{k}_1 d\omega_1 D^{(2)}(\mathbf{k},\mathbf{k}_1;\omega,\omega_1)\phi_\alpha(\mathbf{k}_1,\omega_1)\phi_\beta(\mathbf{k}-\mathbf{k}_1,\omega-\omega_1) \qquad (2.2)$$

and

$$\mathrm{Im}\, M_3(\mathbf{k},\omega) = \sum_{\alpha,\beta,\gamma} \int\int\int\int d\mathbf{k}_1 d\mathbf{k}_2 d\omega_1 d\omega_2 D^{(3)}(\mathbf{k},\mathbf{k}_1,\mathbf{k}_2;\omega,\omega_1,\omega_2)\times$$
$$\phi_\alpha(\mathbf{k}_1,\omega_1)\phi_\beta(\mathbf{k}_2,\omega_2)\phi_\gamma(\mathbf{k}-\mathbf{k}_1-\mathbf{k}_2,\omega-\omega_1-\omega_2) \qquad (2.3)$$

Here, the ϕ's are the spectral functions of individual modes, which are labelled by Greek suffixes for the various branches, and the D's are complicated kernels representing vertex functions.

As already indicated in the introduction, we shall not attempt a quantitative evaluation of these expressions. We shall instead assume that the spectral functions in the integrals (2.2) and (2.3) can be replaced by those of undamped vibrations, i.e.

$$\phi_\alpha(\mathbf{k},\omega) = A_{\mathbf{k}\alpha}\,\delta(\omega - \Omega_\alpha(\mathbf{k})) + B_{\mathbf{k}\alpha}\,\delta(\omega + \Omega_\alpha(\mathbf{k})) \qquad (2.4)$$

where $\Omega_\alpha(\mathbf{k})$ denotes the mode eigenfrequency. This assumption will reduce eqns (2.2) and (2.3) to forms involving densities of states for the transition, thus allowing us to examine the conditions under which one can obtain a large contribution to the microscopic low-frequency conductivity for $\mathbf{k}$ along the [100] direction.

2.1 Two-mode processes

Using eqn (2.4) in eqn (2.2), integrating over ω_1 and writing the integral over $\mathbf{k}_1$ as an integral over constant-frequency surfaces times an integral over the orthogonal component $k_\perp$, that is

$$\int d\mathbf{k} \;\rightarrow\; \int\int \frac{dS_\omega\, d\omega}{\left|\frac{\partial\omega}{\partial k}\right|} \qquad (2.5)$$

we easily find that each of the four contributions to the memory function involves in the integrand factors of the form

$$\left|\frac{\partial}{\partial k_1}[\,\Omega_\alpha(\mathbf{k}_1) \pm \Omega_\beta(\mathbf{k}-\mathbf{k}_1)\,]\right|^{-1} \delta(\Omega_\alpha(\mathbf{k}_1) \pm \Omega_\beta(\mathbf{k}-\mathbf{k}_1) - \omega)$$

Conservation of momentum to within a reciprocal lattice vector has been left implicit.

Clearly, large contributions to the microscopic conductivity at frequencies much below phonon frequencies could arise in this channel from pairs of mode branches at $\mathbf{k}_1$ and $\mathbf{k}-\mathbf{k}_1$, having flat dispersion curves at essentially the same frequency. This consideration immediately draws attention to the optic modes, and in particular to the Raman-active modes (see section 3 below). We should consider, however, that decay processes involving a pair of transverse modes are forbidden in this channel by time reversal symmetry [6] and that simultaneous Bragg scattering would be needed when $\mathbf{k}$ has the value indicated by the QES experiments. We therefore turn to examine the three-mode channel, still within the same energy and momentum conservation and van Hove singularity arguments. The discussion below will indicate that this channel is more probable than the two-mode channel that we have been discussing so far, at least in relation to the QES evidence of present interest.

2.2 Three-mode processes

Use of eqn (2.4) in eqn (2.3) immediately yields the memory function at frequency $\omega \approx 0$ as a sum of contributions which are sixfold integrals in momentum space, involving delta functions for energy conservation in the form

$$\Omega_\alpha(\mathbf{k}_1) \pm \Omega_\beta(\mathbf{k}_2) \pm \Omega_\gamma(\mathbf{k}_3) = 0 \qquad (\mathbf{k}_3 = \mathbf{k}-\mathbf{k}_1-\mathbf{k}_2) \qquad (2.6)$$

However, the integration over momenta will smear out the effect of van Hove singularities unless the sixfold integral can be reduced by suitable restrictions to a single integral.

This is easily achieved, for $\mathbf{k}$ along the [100] direction, by asking that only one of the three wave vectors in eqn (2.6) be along the same direction while the other two are along the [110] and [1$\bar{1}$0] directions. In order to see this, let us write $\mathbf{k} = (k, 0, 0)$, $\mathbf{k}_1 = (\xi_1, 0, 0)$, $\mathbf{k}_2 = (\xi_2, \eta_2, \zeta_2)$ and $\mathbf{k}_3 = (\xi_3, -\eta_2, -\zeta_2)$, with the condition $\xi_1 + \xi_2 + \xi_3 = k$ leaving four independent integration variables. These reduce to two if we ask that the four vectors be colinear, i.e. set $\eta_2 = \zeta_2 = 0$. However, if we ask that $\mathbf{k}_2$ and $\mathbf{k}_3$ be along

the [110] and [1$\bar{1}$0] directions, we have three additional restrictions, i. e. $\xi_2 = \eta_2 = \xi_3$ and $\zeta_2 = 0$, leaving only one independent integration variable (ξ_1, say). The integrands can finally be rewritten to display factors of the form

$$\left| \frac{\partial}{\partial k_1} [\, \Omega_\alpha(\mathbf{k}_1) \pm \Omega_\beta(\mathbf{q}) \pm \Omega_\gamma(\mathbf{q}') \,] \right|^{-1} \delta(\Omega_\alpha(\mathbf{k}_1) \pm \Omega_\beta(\mathbf{q}) \pm \Omega_\gamma(\mathbf{q}'))$$

where $\mathbf{q}$ and $\mathbf{q}'$ are vectors along the [110] and [1$\bar{1}$0] directions, with modulus $|\mathbf{q}| = |\mathbf{q}'| = |\mathbf{k} - \mathbf{k}_1| / (2)^{1/2}$.

In summary, the foregoing discussion indicates that important contributions to the QES cross section, for $\mathbf{k}$ along the [100] direction and well away from the Brillouin zone centre, may come from processes involving three phonons which have the following characteristics: (i) their wave vectors are along the [100], [110] and [1$\bar{1}$0] directions; (ii) their frequencies lie in flat regions of the dispersion curves; and (iii) the three frequencies add to essentially zero when combined in the manner shown by energy conservation in eqn (2.6). We shall proceed in the next section to try to identify triplets of vibrational modes which satisfy the restrictions listed above, using measured dispersion curves of lattice vibrations for fluorite-type materials.

3. Identification of three-mode channels from phonon dispersion curves

The phonon dispersion curves in fluorite-type materials, as measured for $SrCl_2$[9], CaF_2[10], SrF_2[11] and BaF_2[12], show a number of common qualitative features. Focussing for our purposes on the [100] and [110] directions, the following features may be mentioned: (i) the highest-lying Raman-active branches, which are the doubly degenerate transverse branch ($TO_{(R)}$) along [100] and the longitudinal branch ($LO_{(R)}$) along [110], are essentially flat throughout the Brillouin zone; (ii) the longitudinal infrared-active branch ($LO_{(IR)}$) is quite flat along [100] and shows a flat minimum along [110] around (0.6, 0.6, 0), where the longitudinal acoustic branch (LA) shows a broad maximum; (iii) the $LO_{(R)}$ branch along [100] shows appreciable dispersion but flattens

near the zone boundary, where it joins with the [110] transverse acoustic branch of Σ_4(A) symmetry (TA_2), which in turn is very flat over an appreciable portion of the [110] direction. The other branches show flatness in the regions of the Brillouin zone where one expects it on rather general grounds, namely on approaching the zone boundary and, for optic modes, near the zone centre.

Combining the above qualitative features of the phonon branches with the insight and restrictions obtained in section 2, we can identify two main three-mode processes which can give important contributions to the observed QES cross section. The first combines the $TO_{(R)}$ modes along [100] with the LA and TA_2 modes along [110] near the zone boundary. The second combines the $LO_{(R)}$ mode near the zone boundary along [100] with the $LO_{(IR)}$ mode and an acoustic mode near the point (0.6, 0.6, 0). From the measured frequencies the acoustic mode entering the second channel is the LA mode in CaF_2, SrF_2 and BaF_2, but the TA_2 mode in $SrCl_2$. For CaF_2, there also is the possibility of combining the $LO_{(R)}$ mode near (0.6, 0.6, 0) with the TA_2 mode near the same point and with the TA mode near (100). The extent to which conservation of momentum and energy is satisfied by the above choices is shown in Table 1.

We have also carried out lattice dynamics calculations in a rigid-ion model for CaF_2 and $SrCl_2$, in order to examine the eigenvectors of the various modes and thus obtain further insight into the microscopic processes that we have pointed out above. An important point is that a Raman-active mode plays a role in all processes and that the corresponding eigenvectors describe displacements in opposite directions for the two halogens in the unit cell, the alkaline earth atoms being immobile. A distinction between the two types of three-mode channels arises from the modes that accompany the $TO_{(R)}$ or the $LO_{(R)}$ mode. In broad terms, however, one may say that the displacements associated with the partner modes describe separation between the halogen and alkaline earth components in all cases. A more precise assessment can be made from the calculated mode eigenvectors, which are given in Table 2. To simplify reading of the Table, we have set equal to zero the components of the eigenvectors that are of order 0.1 or less.

4. Discussion

Hutchings et al [4] have interpreted their QES data, in conjunction with neutron diffraction data, by means of a model which invokes short-lived defect clusters comprising anion Frenkel interstitials, anion vacancies and relaxed anions. Their interpretation suggests a concentration of Frenkel defects of the order of 5% at the temperature T_c marked by the peak in the heat capacity which accompanies the diffuse superionic transition in fluorites. The foregoing discussion throws some light on the microscopic dynamical processes that will lead to the formation of such defects and defect clusters as the crystal is heated towards T_c.

The closest analogue to our work is perhaps the discussion given by Bührer and Brüesch[13] for the superionic transition in AgI, that they related to the presence of a low-frequency optic mode in the low-temperature ordered phase. This mode in AgI shows a flat dispersion and favours the promotion of a cation to an interstitial site, thus acting as a precursor of the cationic order-disorder transition in this material.

The dynamical picture that we have proposed for the precursors of the fast-ion conduction state in fluorites is less simple, a possible reason for this being that the superionic transition in these materials is not accompanied by a structural phase transition as in AgI. Nevertheless, we have been able to point out a major role for the Raman-active modes, assisted by coupling to various other modes. Although we have reached this conclusion on the sole basis of the QES evidence, we may emphasize at this point that strong couplings between these modes will also lead to their broadening across the transition, thus making our interpretation consistent with the rest of the available dynamical evidence that we have quoted at the start of this work. Finally, our calculation of atomic displacements in the precursor modes indicates that they tend to favour the formation of anionic disorder of the type proposed by Hutchings et al.

Acknowledgments. One of the authors (D. K. C.) wishes to thank Professor Abdus Salam, the International Atomic Energy Agency and UNESCO for hospitality at the International Centre for Theoretical Physics in Trieste, where this work was partly carried out during the Condensed Matter Theory Workshops of 1986 and 1987. The other author acknowledges sponsorship by the Ministero della Pubblica Istruzione and the Consiglio Nazionale delle Ricerche of Italy and the collaboration of Dr U. Marini Bettolo Marconi in the early stages of this work.

REFERENCES

1. M. H. Dickens, M. T. Hutchings and J. B. Suck, Solid State Commun. **34**, 559 (1980).
2. R. J. Elliott, W. Hayes, W. G. Kleppman, A. J. Rushworth and J. F. Ryan, Proc. Roy. Soc. **A360**, 317 (1978).
3. K. Clausen, W. Hayes, M. T. Hutchings, J. K. Kjems, P. Schnabel and C. Smith, Solid State Ionics **5**, 589 (1981).
4. M. T. Hutchings, K. Clausen, M. H. Dickens, W. Hayes, J. K. Kjems, P. Schnabel and C. Smith, J. Phys. **C17**, 3903 (1984).
5. H. Mori, Progr. Theor. Phys. **33**, 423 (1965); **34**, 399 (1965).
6. D. K. Chaturvedi, U. Marini Bettolo Marconi and M. P. Tosi, Nuovo Cimento **57B**, 319 (1980).
7. J. Bosse and T. Munakata, Phys. Rev. **A25**, 2763 (1982); T. Munakata and J. Bosse, Phys. Rev. **A27**, 455 (1983).
8. L. Sjögren and F. Yoshida, J. Chem. Phys. **77**, 3703 (1982).
9. A. Sadoc, F. Moussa and G. Pepy, J. Phys. Chem. Solids **37**, 197 (1976).
10. M. M. Elcombe and A. W. Pryor, J. Phys. **C3**, 492 (1970).
11. M. M. Elcombe, J. Phys. **C5**, 2702 (1972).
12. J. P. Hurrell and V. J. Minkiewicz, Solid State Commun. **8**, 463 (1970)
13. W. Bührer and P. Brüesch, Solid State Commun. **16**, 155 (1975).

Table 1. Frequencies of selected vibrational modes at the indicated wave vectors in fluorite-type materials (THz)

CaF_2:								
	$TO_{(R)}$(0.4, 0, 0):	9.8	LA(1, 1, 0):	5.7	TA_2(1, 1, 0):	4.5		
	$LO_{(R)}$(1, 0, 0):	4.5	$LO_{(IR)}$(0.6, 0.6, 0):	11.4	LA(0.6, 0.6, 0):	7.7		
	$LO_{(R)}$(0.6, 0.6, 0):	10.0	TA_2(0.6, 0.6, 0):	4.7	TA(1, 0, 0):	5.3		
SrF_2:								
	$TO_{(R)}$(0.4, 0, 0):	8.3	LA(1, 1, 0):	4.5	TA_2(1, 1, 0):	3.8		
	$LO_{(R)}$(1, 0, 0):	4.6	$LO_{(IR)}$(0.6, 0.6, 0):	10.0	LA(0.6, 0.6, 0):	5.4		
BaF_2:								
	$TO_{(R)}$(0.4, 0, 0):	7.3	LA(1, 1, 0):	4.5	TA_2(1, 1, 0):	3.0		
	$LO_{(R)}$(1, 0, 0):	4.6	$LO_{(IR)}$(0.6, 0.6, 0):	8.3	LA(0.6, 0.6, 0):	4.0		
$SrCl_2$:								
	$TO_{(R)}$(0.4, 0, 0):	5.5	LA(1, 1, 0):	2.5	TA_2(1, 1, 0):	3.0		
	$LO_{(R)}$(1, 0, 0):	3.0	$LO_{(IR)}$(0.6, 0.6, 0):	5.9	TA_2(0.6, 0.6, 0):	3.0		

Table 2. Approximate values of relevant mode eigenvectors for $SrCl_2$

	e(Cl_1)	e(Cl_2)	e(Sr)
$TO_{(R)}$(0.4, 0, 0):	(0, 0, 0.7)	(0, 0, -0.7)	(0, 0, 0)
LA(1, 1, 0):	(0, 0, 0)	(0, 0, 0)	(0.5, 0.9, 0)
TA_2(1, -1,0):	(0, 0, 0.7)	(0, 0, 0.7)	(0, 0, 0)
$LO_{(R)}$(1, 0, 0):	(0.7, 0, 0)	(-0.7, 0, 0)	(0, 0, 0)
$LO_{(IR)}$(0.6, 0.6, 0):	(0.5, 0.5, 0)	(0.5, 0.5, 0)	(0, 0, 0)
TA_2(0.6, -0.6, 0):	(0, 0, 0.7)	(0, 0, 0.7)	(0, 0, 0)